



# City Research Online

## City, University of London Institutional Repository

---

**Citation:** Liu, F., Andrienko, G. ORCID: 0000-0002-8574-6295, Andrienko, N. ORCID: 0000-0003-3313-1560, Chen, S., Janssens, D., Wets, G. and Theodoridis, Y. (2020). Citywide Traffic Analysis Based on the Combination of Visual and Analytic Approaches. *Journal of Geovisualization and Spatial Analysis*, 4(2), 15.. doi: 10.1007/s41651-020-00057-4

This is the accepted version of the paper.

This version of the publication may differ from the final published version.

---

**Permanent repository link:** <https://openaccess.city.ac.uk/id/eprint/26087/>

**Link to published version:** <http://dx.doi.org/10.1007/s41651-020-00057-4>

**Copyright:** City Research Online aims to make research outputs of City, University of London available to a wider audience. Copyright and Moral Rights remain with the author(s) and/or copyright holders. URLs from City Research Online may be freely distributed and linked to.

**Reuse:** Copies of full items can be used for personal research or study, educational, or not-for-profit purposes without prior permission or charge. Provided that the authors, title and full bibliographic details are credited, a hyperlink and/or URL is given for the original metadata page and the content is not changed in any way.

---

City Research Online:

<http://openaccess.city.ac.uk/>

[publications@city.ac.uk](mailto:publications@city.ac.uk)

---

## Citywide traffic analysis based on the combination of visual and analytic approaches

Feng liu<sup>a,b</sup>, Gennady Andrienko<sup>c</sup>, Natalia Andrienko<sup>c</sup>, Siming Chen<sup>c</sup>, Davy Janssens<sup>a</sup>, Geert Wets<sup>a</sup>, Yannis Theodoridis<sup>d</sup>

<sup>a</sup> Transportation Research Institute (IMOB), Hasselt University, Wetenschapspark 5, bus 6, B-3590, Diepenbeek, Belgium

<sup>c</sup> Fraunhofer Institute IAIS - Intelligent Analysis and Information Systems, Schloss Birlinghoven, Sankt-Augustin, D-53757 Germany

<sup>d</sup> University Piraeus, 80 Karaoli & Dimitriou Str., GR-18534 Athens, Greece

[Feng.liu@uhasselt.be](mailto:Feng.liu@uhasselt.be) (Feng liu), [gennady.andrienko@iais.fraunhofer.de](mailto:gennady.andrienko@iais.fraunhofer.de) (Gennady Andrienko), [Natalia.andrienko@iais.fraunhofer.de](mailto:Natalia.andrienko@iais.fraunhofer.de) (Natalia Andrienko), [Siming.Chen@iais.fraunhofer.de](mailto:Siming.Chen@iais.fraunhofer.de) (Siming Chen), [davy.janssens@uhasselt.be](mailto:davy.janssens@uhasselt.be) (Davy Janssens), [geert.wets@uhasselt.be](mailto:geert.wets@uhasselt.be) (Geert Wets), and [ytheodoridis@gmail.com](mailto:ytheodoridis@gmail.com) (Yannis Theodoridis)

<sup>b</sup> Corresponding author: Tel: +32 0 11269125 fax: +32 0 11269199

### Compliance with Ethical Standards

Funding: The work was sponsored by the EU Horizon 2020 research and innovation program Grant 780754.

Conflict of Interest: The authors declare that they have no conflict of interest.

Ethical Approval: This paper does not contain any studies with human participants or animals performed by any of the authors.

Informed Consent: Informed consent was obtained from all individual participants included in the study.

# Citywide traffic analysis based on the combination of visual and analytic approaches

## Abstract

A method for citywide traffic analysis is introduced based on the combination of visual and analytical approaches. Large volumes of GPS data collected from urban vehicles are utilized. In the method, a traffic-condition-map is constructed, composed of five different layers featuring traffic conditions, road linkage, travel patterns, congestion zones and traffic flows, respectively. Based on the map, specific transport situations surrounding the congested areas are examined and ways of reducing congestion are suggested. The method is evaluated in the aggregated metropolitan area of Athens and Piraeus in Greece, and the potential and the effectiveness of this technique in analyzing traffic are demonstrated. With more and more urban vehicles being equipped with GPS devices, the method can be easily transferable to other regions, paving the way for the adoption of the approach for an up-to-date, spatial-temporal sensitive, visual and analytic method for traffic monitoring that supports the establishment of a more sustainable urban transportation system.

Keywords visual analytical approaches, traffic conditions, travel patterns, congestion, GPS data

## 1 Introduction

Batty (2013) considers a city as a system composed of movement flows (between locations and between activities), networks of relationships, and interactions among various entities. For understanding the urban movement flows and traffic, both *visual analytical approaches (VAA)* and *statistical and algorithmic approaches (SAA)* have been developed. The methods analyze a variety of *big mobility data*, including GPS (Global Positioning Systems) (e.g. Chen et al. 2019; Liu et al. 2019), mobile phone (e.g. Skupin 2013), smart card (e.g. Itoh et al. 2016), and space- and time-referenced social media (e.g. Chae et al. 2014; Lansley and Longley 2016) data. Big mobility data (particularly GPS data) offer detailed movement trajectories, enabling the examination of urban mobility in highly spatial-temporal resolution and across a large part of the transport network, having great potential in supporting policies.

However, while a multitude of VAA and SAA has been adopted for mobility and traffic analysis, there are few studies on the combination of these two types of approaches. The existing VAA (and their implementation software programs) are usually manageable for a limited size of data (e.g. a few gigabytes (GB)), but would be very slow or even fail when being applied to extremely large volumes of data (e.g. dozens of GB). Image processing requires a lot of memories, and displays even on a middle level of resolution cannot show millions or even billions of movement points at the same time without completely cluttering the screen (e.g. Andrienko et al. 2013b). Thus, SAA, which are capable of

efficiently processing a large size of data, are sorely needed to reduce the data volume by data aggregation and selection, and to bring out the important properties. However, such statistical and algorithmic methods, though being able to generate tables and figures or to display the analytical results on a dynamic map (e.g. in a route planner), they are inefficient in enabling interactive exploration of the analytical process under various parameter settings and scenarios. The methods also have limitations in supporting traffic managers to maximally utilize the derived results for gaining more insights and designing more effective policy measures. This is exactly the challenge, and if a methodology (or a process) can be found which tightly integrates the VAA and SAA techniques into a common development framework, the integrated method would utilize the strength of both approaches and enable urban mobility and traffic analysis in an interactive manner while based on large volumes of GPS data.

To this end, a visual and analytical method combining both VAA and SAA techniques has been developed in this paper, with the goal of interactively systematic examining traffic conditions and analyzing congestion problems across the entire urban area. Compared to existing VAA and SAA, the proposed method offers the following advantages. (1) It integrates VAA and SAA into a common framework, enabling visual and analytical analysis on urban traffic based on large sizes of GPS data. (2) The visualization allows interactive inspection into traffic situations, facilitating analysts and traffic managers acquiring more insights during the development process of the approach and the exploration of the derived results. (3) Due to the utilization of massive data, the derived results are more objective and representative. (4) A unique citywide traffic-condition-map is constructed, comprised of five different layers featuring key aspects (i.e. traffic conditions, road linkage, travel patterns, congestion zones and traffic flows) of the road network respectively. This enables comprehensive analysis on urban traffic by means of various combinations of these layers. (5) Specific transport situations surrounding the congestion areas are examined and ways of reducing congestion are suggested.

The rest of this paper is organized as follows. Section 2 gives literature reviews, while Section 3 details the proposed method. A case study is performed in Section 4, and finally Section 5 ends this paper with major discussions and conclusions.

## 2 Literature reviews

### 2.1 Visual analytics for urban mobility analysis

*The science of visual analytical approaches develops principles, methods and tools to enable synergistic work between humans and computers through interactive visual interfaces* (Thomas and Cook 2005). Such interfaces support the unique capabilities (e.g. flexible application of prior knowledge and experiences, creative thinking, and insights) of humans, and couple these capabilities with machines'

computational strength, enabling the generation of new knowledge from large volumes of and complex data recorded from urban areas (e.g. Xie et al. 2019).

Various VAA have been developed, and they explore mobility and mobility-related phenomena from different perspectives. A review by Andrienko and Andrienko (2013a) considered approaches *from the data processing perspective*. It includes analyzing individual trajectories (e.g. trajectory cleaning and clustering), and transforming trajectories into data of various spatial-temporal resolution. A more recent review (Andrienko et al. 2017) outlined approaches *from the travel and driving behavior perspective*. In terms of travel behavior, it consists of understanding the details of individual movement traces and the variety of taken routes; assessing the dynamics of aggregated movement of a group along routes of a single road, between origins and destinations, or across the entire study area. With respect to driving behavior, the review describes methods of detecting movement events (e.g. harsh brakes and sharp turns) and analyzing the context, impact and risk of the events. Moreover, Markovic et al. (2019) presented a viewpoint *from the traffic modelling and management perspective*, specifying the following problems of interest: estimating travel demand, analyzing and predicting traffic conditions, designing public transit, improving road safety, and assessing impact of traffic on the environment.

## 2.2 Statistical and algorithmic approaches on traffic studies

Alongside visual analytics, there is rich literature on statistical and algorithmic approaches for urban mobility and traffic studies based on big mobility data. The most commonly used technique is *Floating Car Data* which employs a number of GPS-equipped vehicles (e.g. taxis) as moving sensors to build *Intelligent Transportation Systems (ITS)*, in order to monitor real-time traffic conditions on the roads and predict short-term traffic evolution (e.g. congestion) (e.g. Dias et al. 2019). The information is further used for dynamic routing and navigation in a route planner (e.g. the google map <https://www.google.be/maps/@50.9304038,5.3372893,12z>). ITS provides a real-time solution to an end-user, enabling individuals to effectively manage the current traffic and optimize the utilization of existing transport network capacities. Apart from real-time analysis, efforts have also been devoted to examine major traffic parameters during a certain time period (e.g. several weeks, months or years) using historical GPS data. The goal is to systematically analyze, uncover and solve traffic problems that are persistent for long time, in order to support long-lasting transport improvement. The typical research includes the followings. Zeng et al. (2019) developed a Cellular Automaton model to estimate traffic flows for single and two lane highways, while Yuan et al. (2011) proposed an approach of deriving travel time of *landmarks* that are road links frequently traversed by taxis. Moreover, Ruan et al. (2019) constructed models of *traffic density* (the number of vehicles per unit length of the roadway) and further predicted

congestion levels and effects of weather on congestion. Cui et al. (2016a) developed urban mobility demand models and detected serious mismatch between mobility demand and road network services, uncovering major causes of congestion in the study area.

### 3 The method

#### 3.1 Overall structure of the method

The method introduced here consists of four major steps: (1) The entire study area is divided into zones, and three matrices characterizing traffic conditions, road linkage and travel patterns of each zone or zone pair are constructed and visualized; (2) Based on the matrices, congestion zones are detected; (3) Major sources of traffic flows in the obtained congestion zones are analyzed; (4) Specific transport situations surrounding the congestion areas are further examined and ways of alleviating congestion are explored. Prior to these steps, a preliminary step is conducted for raw GPS data preprocessing and trip extraction.

To realize the above steps, two components, including *a VAA* and *a SAA components*, are adopted, accommodating the VAA and SAA techniques respectively. In the preliminary step, the VAA component is applied to *a small sample dataset* drawn from *the entire dataset* (the whole data used in the analysis), in order to interactively examine the data, extract rules for removing data errors, and specify parameter values for trip extraction. Based on these results, the entire dataset is cleaned and trips are derived in the SAA component. In the next steps (Steps 1-3), three matrices for traffic conditions, road linkage and travel patterns are constructed using the obtained trips in SAA, and congestion zones and major sources of traffic flows in the congestion areas are further recognized. All the results are then transferred to VAA, in which they are visualized on different layers of *a map (the traffic-condition-map)*. In the last step, specific transport situations surrounding the congestion zones are further examined based on the map, and ways of alleviating congestion are investigated. The connection between the two components includes 4 parts: the extracted rules; the three matrices; the detected congestion zones; and the major sources of traffic flows in the congestion zones. The first part (the extracted rules) is linked from VAA to SAA through knowledge transfer, while the last three parts (the computed results) are connected from SAA to VAA by means of data transfer (i.e. by external files of CSV or XML). The overall structure of the method is shown in Fig. 1, where the connection points (parts) between VAA and SAA are indicated with the red solid arrows between the two components.

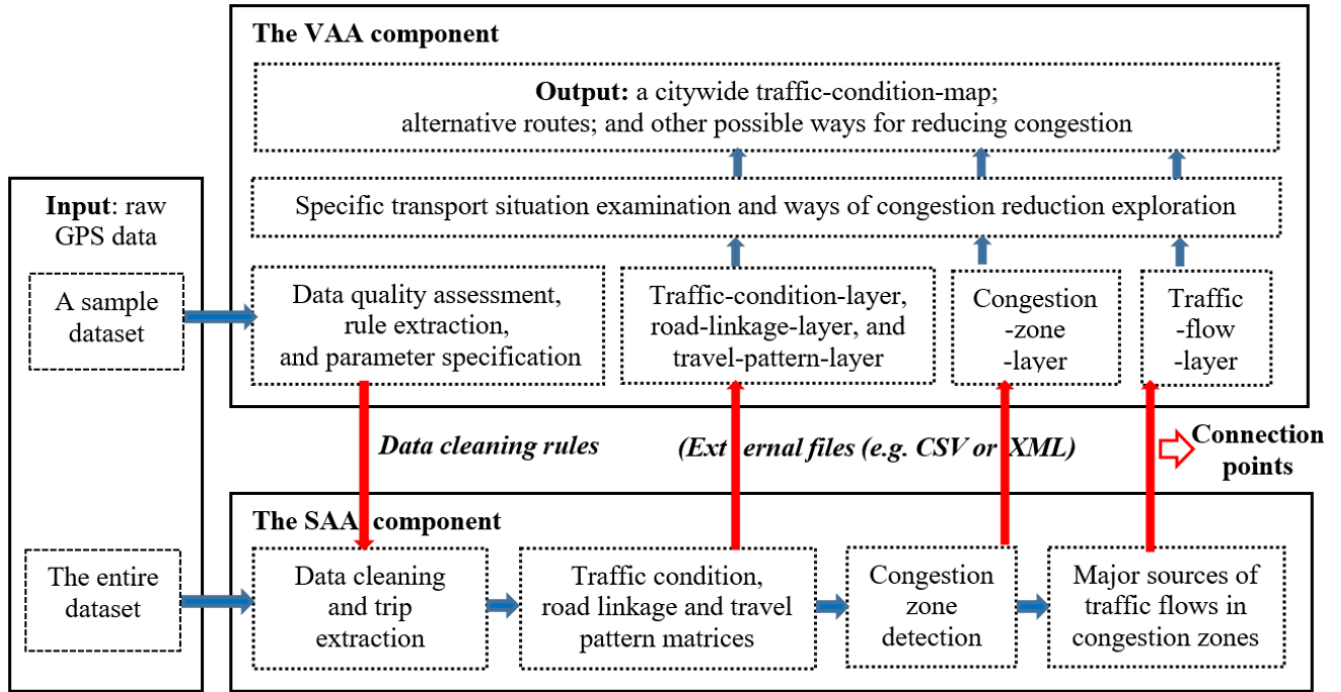


Fig. 1 Overall structure of the method

### 3.2 GPS data preprocessing and trip extraction

#### 3.2.1 Rule extraction and parameter specification in VAA

**Definition 2.1:** A GPS trajectory from a vehicle can be described as a sequence of time-ordered GPS points, i.e.  $Tra = p_1(id_1, L_1, t_1, a_1) - \dots - p_K(id_K, L_K, t_K, a_K)$ ; where  $p_k$  ( $k=1 \dots K$ ) represents a point with its identification (ID) as  $id_k$ , longitude and latitude as  $L_k=(X_k, Y_k)$ , time stamp as  $t_k$ , and attributes as  $a_k$  (e.g. instant speed  $v_k$  and heading  $h_k$ ), and  $K$  is the total number of the points.

Raw GPS data usually contain bad records caused by random errors (e.g. clouding); the existing visual analytical approach on data quality assessment and trip extraction (Andrienko et al. 2016) is adopted. In the method, errors that may occur in all aspects of the data, namely time and space (e.g. time intervals and distances between two consecutive points) and other attributes (e.g. instant speeds and headings), are examined. For trip extraction, the following steps are undertaken.

- 1) For a group of consecutive points, e.g.  $p_i(id_i, L_i, t_i, a_i) - \dots - p_j(id_j, L_j, t_j, a_j)$  ( $j > i$ ), if each of the points has  $v_k = 0$  ( $k=i \dots j$ ) and if the stop duration  $t_{stop}$  ( $t_{stop} = t_j - t_i$ ) is longer than a parameter  $TH_{Act}$ , the points are clustered into a *stop-location* where the person stays for doing activities.
- 2) The points in between two adjacent stop-locations are extracted as a candidate trip; if the distance (computed according to Formula 1) between the first and last points of the trip is larger than a threshold  $TH_{Trip}$ , the trip is retained.



The above method is applied to the sample dataset, by which data errors are identified and rules for eliminating these errors are generated. Moreover, appropriate values for  $TH_{Act}$  and  $TH_{Trip}$  are set up.

### 3.2.2 Data cleaning and trip derivation in SAA

Based on the above-derived rules and parameter settings, the entire dataset is cleaned and trips are derived in SAA. For each of the obtained trips, i.e.  $Trip = p_s(id_s, L_s, t_s, a_s) - \dots - p_m(id_m, L_m, t_m, a_m) - \dots - p_n(id_n, L_n, t_n, a_n) - \dots - p_e(id_e, L_e, t_e, a_e)$  ( $s \leq m < n \leq e$ ), the travel time  $t_{mn}$ , travel distance  $d_{mn}$ , and travel speed  $v_{mn}$  of the segment of the trip between  $p_m$  and  $p_n$  are computed as follows.

$$\begin{aligned}
 t_{mn} &= t_n - t_m \\
 d_{mn} &= \sum_{k=m}^{n-1} [D(p_k, p_{k+1})] \\
 v_{mn} &= \frac{d_{mn}}{t_{mn}}
 \end{aligned} \tag{1}$$

Where,  $D(p_k, p_{k+1})$  is the geographic distance between two consecutive points  $p_k$  and  $p_{k+1}$  derived from the Haversine formula ([https://en.wikipedia.org/wiki/Haversine\\_formula](https://en.wikipedia.org/wiki/Haversine_formula)).

## 3.3 Citywide traffic condition, road linkage and travel pattern characterization

### 3.3.1 Study area division and trip projection in SAA

The entire study area is divided into  $Grid\_X \times Grid\_Y$  disjoint zones using a grid-based method, with each zone being identified as  $Z_i$  ( $i=1, \dots, Grid\_X \times Grid\_Y$ ) or  $Z_{i_1, i_2}$  ( $i_1=1, \dots, Grid\_X$  and  $i_2=1, \dots, Grid\_Y$ ). The temporal dimension is classified into different *time periods of a day* ( $TimeP$ ) and different *types of the day* ( $DayT$ ), including weekdays, weekends and public holidays. Based on the spatial and temporal division, each point of each trip is projected into the corresponding zones and time periods.

Definition 2.2 For each trip  $Trip = p_s(id_s, L_s, t_s, a_s) - \dots - p_e(id_e, L_e, t_e, a_e)$ , all the GPS points along the trace are matched into zones, generating a trip at the zone level as  $Trip\text{-}zone = Z_s(t_s) - \dots - Z_e(t_e)$ , with  $Z_i$  ( $i=s \dots e$ ) referring to the corresponding zone. Moreover, the consecutive zones that are identical are further combined, leading to a *travel path* of the trip, i.e.  $Path = Z_s - \dots - Z_e$ , with  $Z_j$  ( $j=s \dots e$ ) denoting the distinct zone passed by the trip (See Fig. 2).

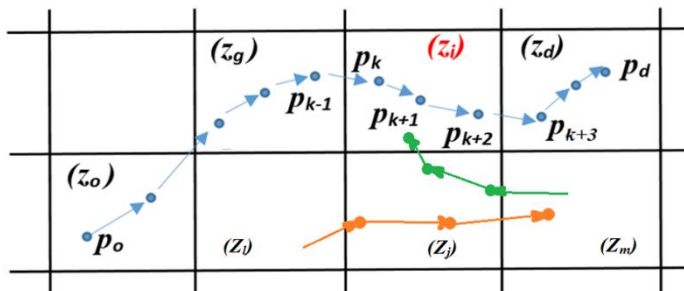


Fig. 2 The zones and trips

Note: the black grids represent zones, the curves are trips, and the dots along the curves denote GPS points. The blue curve (trip) starts and ends at  $p_o$  and  $p_d$  respectively, covering 4 zones of  $Z_o, Z_g, Z_i$  and  $Z_d$ , i.e.  $Path=Z_o-Z_g-Z_i-Z_d$ . For  $TC$ , the segment of the trip traversing  $Z_i$  (in red) is between  $p_k$  and  $p_{k+3}$ ; for  $RL$ , the segment passing  $Z_o, Z_g$  and  $Z_i$  is between  $p_o$  and  $p_{k+3}$ ; for  $TP$ , the entire trip between  $p_o$  and  $p_d$  is adopted. Moreover, the orange and green trips describe the trip segment traversing  $Z_i, Z_j$  and  $Z_m$  as well as  $Z_m, Z_j$  and  $Z_i$ , indicating the existence of road connectivity  $Z_l \rightarrow Z_j \rightarrow Z_m$  and  $Z_m \rightarrow Z_j \rightarrow Z_i$ , respectively. However, these two connections are not linked inside  $Z_j$ , leading to the absence of the connectivity  $Z_l \rightarrow Z_j \rightarrow Z_i$ .

### 3.3.2 Matrix construction in SAA

Based on the *Trip-zone* or *Path* of all the trips, three matrices characterizing traffic conditions, road linkage and travel patterns of the study area are constructed respectively. First, *the traffic-condition-matrix*  $TC(Z_i, TimeP, Day, DayT)$  accommodates all trip segments that traverse each zone  $Z_i$  within  $TimeP$  on the  $Day$  with the type of  $DayT$ . Two variables are derived for each matrix element, including the total number ( $M_i$ ) of trip segments that traverse  $Z_i$  during the time of  $TimeP, Day$  and  $DayT$ , and the average travel speed ( $V_i$ ) over all the segments. The latter variable is computed by Formula 2.

$$V_i = \frac{\sum_{w=1}^{M_i} v_{m'n^{(w)}}}{M_i} \quad (2)$$

Where,  $w$  represents a trip that passes  $Z_i, p_{m'}$  and  $p_{n'}$  are the first points of the trip in  $Z_i$  and out of  $Z_i$  respectively (See Fig. 2), and  $v_{m'n^{(w)}}$  is the speed of the segment between  $p_{m'}$  and  $p_{n'}$  (See Formula 1).

Secondly, *the road-linkage-matrix*  $RL(Z_i, Z_j, Z_l, TimeP, Day, DayT)$  describes trip segments that successively pass three zones of  $Z_i, Z_j$  and  $Z_l$  in  $TimeP$  on the  $Day$  of  $DayT$ . Two features are extracted for each matrix element, including the total number ( $M_{ijl}$ ) of the segments and the average speed ( $V_{ijl}$ ) over the segments.  $V_{ijl}$  is computed according to Formula 3.

$$V_{ijl} = \frac{\sum_{w=1}^{M_{ijl}} v_{m''n''^{(w)}}}{M_{ijl}} \quad (3)$$

Where,  $w$  represents a trip that passes  $Z_i, Z_j$  and  $Z_l, p_{m''}$  and  $p_{n''}$  are the first points of the trip in  $Z_i$  and out of  $Z_l$  respectively (See Fig. 2), and  $v_{m''n''^{(w)}}$  is the speed of the segment between  $p_{m''}$  and  $p_{n''}$ .  $RL$  characterizes *road connectivity* ( $Z_i \rightarrow Z_j \rightarrow Z_l$ ) between  $Z_i, Z_j$  and  $Z_l$ , with the value of  $M_{ijl}$  larger than 0 signifying the existence of road connections (in the corresponding direction) among these zones. It should be noted that, despite the existence of road connections among three neighbouring zones, e.g.  $Z_l \rightarrow Z_j \rightarrow Z_m$  among  $Z_l, Z_j$  and  $Z_m$  and  $Z_m \rightarrow Z_j \rightarrow Z_i$  among  $Z_m, Z_j$  and  $Z_i$ , these two connections may not be linked inside the middle zone  $Z_j$ , leading to the absence of the connectivity  $Z_l \rightarrow Z_j \rightarrow Z_i$ , as illustrated in Fig. 2.

Thirdly, *the travel-pattern-matrix*  $TP(Z_o, Z_d, r, TimeP, Day, DayT)$  represents all trips that originate from  $Z_o$ , end in  $Z_d$ , travel along the  $r^{th}$  distinct path, and start within  $TimeP$  on the  $Day$  of  $DayT$ . Let  $Num_{od}$  be the total number of the distinct paths, thus  $r=1 \dots Num_{od}$ . Each element of the matrix is

characterized with five variables, including the travel path ( $Path_{odr}$ ), the total number ( $M_{odr}$ ) of trips along the path, and the average travel speed ( $V_{odr}$ ), travel distance ( $L_{odr}$ ) and travel time ( $T_{odr}$ ) over the trips.  $V_{odr}$ ,  $L_{odr}$  and  $T_{odr}$  are obtained as follows.

$$V_{odr} = \frac{\sum_{w=1}^{M_{odr}} v_{m''''n''''(w)}}{M_{odr}} \quad (4)$$

$$L_{odr} = \frac{\sum_{w=1}^{M_{odr}} d_{m''''n''''(w)}}{M_{odr}}$$

$$T_{odr} = \frac{\sum_{w=1}^{M_{odr}} t_{m''''n''''(w)}}{M_{odr}}$$

Where,  $v_{m''''n''''(w)}$ ,  $d_{m''''n''''(w)}$  and  $t_{m''''n''''(w)}$  are the travel speed, travel distance and travel time of the entire trip  $w$  (i.e. between the first and last points of  $p_{m''''}$  and  $p_{n''''}$ ) respectively (See Fig. 2).

### 3.3.3 Matrix visualization in VAA

Once the matrices are constructed, they are imported and visualized in VAA. Specifically, for a chosen time period and day (or day type), the variables from each of the matrices, including  $M_i$  and  $V_i$  from  $TC$ ,  $M_{ijl}$  and  $V_{ijl}$  from  $RL$ , and  $Path_{odr}$ ,  $M_{odr}$ ,  $V_{odr}$ ,  $L_{odr}$  and  $T_{odr}$  from  $TP$ , are visualized on three different layers (including *the traffic-condition-layer*, *road-linkage-layer* and *travel-pattern-layer*) of the traffic-condition-map respectively, for a part or the entire study area.

## 3.4 Detection of congestion zones

### 3.4.1 Congestion zone detection in SAA

To detect congestion zones, the method proposed in the literature (Cui et al. 2016a; Zheng et al. 2011) is adopted. This approach consists of two steps; the first is to identify zones with congestion each day, while the second is examine the occurrence probability of the daily congestion over all observation days. The aim is to detect zones that regularly suffer from traffic problems.

(1) To detect congestion on a day, the zones with  $M_i > TH_{mz}$  and  $V_i < TH_{vz}$  are selected, where  $M_i$  and  $V_i$  are the number of trip segments and average speed of the segments in  $Z_i$  during  $TimeP$  of the day, and  $TH_{mz}$  and  $TH_{vz}$  are the thresholds for the minimum number of trips and lowest speed in normal traffic situations in  $TimeP$ , respectively. The condition  $M_i > TH_{mz}$  ensures that the detected zones have a high volume of traffic and they thus may accommodate important travel corridors or activity locations (e.g. high-density residence, employment, shopping and/or leisure areas). This high volume also enables the value of  $V_i$  to be more accurate and better represent the traffic conditions of the corresponding zones.

(2) To differentiate the situations between temporary congestion for only one or several days caused by anomaly events (e.g. traffic accidents or road construction work), and systematic problems that remain for long time and constantly cause poor transport performance, *the occurrence probability* ( $P_i$ ) of the congestion in  $Z_i$  over all the observation days of the same type is further computed by Formula 5.

$$P_i = \frac{\sum_{Day=1}^{Num(DayT)} I(M_i > TH_{mz} \text{ and } V_i < TH_{vz})}{N(DayT)} \quad (5)$$

Where,  $Num(DayT)$  denotes the total number of the days of  $DayT$ .  $I(x)$  is a Boolean function with  $x$  as the logical parameter;  $I=1$  if  $x=true$  and  $I=0$  if otherwise. The zone with  $P_i$  larger than a threshold  $TH_{con}$  is chosen as a *congestion zone*, referred as  $Z_{con}(TimeP, DayT)$ .

### 3.4.2 Congestion zone visualization in VAA

All the detected congestion zones are visualized on the 4<sup>th</sup> layer (*congestion-zone-layer*) of the map, showing the geographic distribution of these areas. Detailed traffic conditions, road connectivity and/or travel patterns of these zones can be observed from the previously constructed layers.

## 3.5 Major sources of traffic flows in the congestion zones

### 3.5.1 Traffic source identification in SAA

**Definition 2.3** Given a congestion zone  $Z_{con}(TimeP, DayT)$ , all trips that start, end or just pass  $Z_{con}$  in  $TimeP$  of  $DayT$  are extracted, and they are further classified based on the OD zones of the trips. In each class, if *the number of trips over the total number of the trips* ( $M_{od-con}$ ) is larger than (or equal to) a threshold  $TH_{od-con}$ , the class is selected. The corresponding OD zones and the most frequently used route of the trips are defined as *a major source of the traffic flows in  $Z_{con}$* , referred as  $Source(Z_{o-con}, Z_{d-con}, Path_{od-con})$ .  $Z_{o-con}$  and  $Z_{d-con}$  represent the OD zones, and  $Path_{od-con}$  is the travel path, i.e.  $Path_{od-con} = Z_{o-con} - \dots - Z_k - \dots - Z_{d-con}$ , with  $Z_{o-con} = Z_{con}$ ,  $Z_{d-con} = Z_{con}$ , or  $Z_k = Z_{con}$  (See Fig. 3).

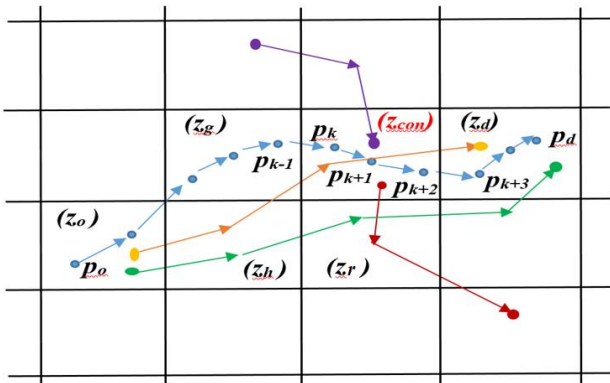


Fig. 3 Major sources of traffic flows in the congestion zone  $Z_{con}$

Note: the black grids represent zones, and the grid  $Z_{con}$  (in red) is the congestion zone. The curves denote the trips; four of which start, end or just pass  $Z_{con}$ , including the red trip starting in  $Z_{con}$  (classified into the 1<sup>st</sup> class), purple trip ending in  $Z_{con}$  (the 2<sup>th</sup> class), and blue and orange trips passing  $Z_{con}$  (the 3<sup>th</sup> class). Let  $TH_{od-con}=0.3$ , the 3<sup>th</sup> class is selected as the major source  $Source(Z_{o-con}, Z_{d-con}, Path_{od-con})$ , with  $Z_{o-con}=Z_o$ ,  $Z_{d-con}=Z_d$ , and  $Path_{od-con}=Z_o-Z_g-Z_{con}-Z_d$  or  $Path_{od-con}=Z_o-Z_h-Z_{con}-Z_d$ . The remaining green trip ( $Path=Z_o-Z_h-Z_r-Z_d$ ) starts and ends in the same zones as this major source but bypassing  $Z_{con}$ , and it is thus chosen as the alternative route between  $Z_o$  and  $Z_d$ .

### 3.5.2 Traffic source visualization in VAA

A 5<sup>th</sup> layer (*traffic-flow-layer*) is constructed, on which all the major sources of traffic flows that start, end or just pass a congestion zone  $Z_{con}$  (upon selected) are shown in terms of  $Z_{o-con}$ ,  $Z_{d-con}$  and  $Path_{od-con}$ .

## 3.6 Specific transport situation examination and ways of congestion reduction exploration in VAA

### 3.6.1 Alternative routes avoiding the congestion zone $Z_{con}$

For each  $Source(Z_{o-con}, Z_{d-con}, Path_{od-con})$  of the flows in  $Z_{con}$ , if  $Z_{o-con} \neq Z_{con}$  and  $Z_{d-con} \neq Z_{con}$ , i.e. if the trips (*passing-trips*) between  $Z_{o-con}$  and  $Z_{d-con}$  just pass  $Z_{con}$  instead of starting or ending in  $Z_{con}$ , we search for *alternative routes* ( $Path_{alter}$ ) that start and end in the same zones as  $Z_{o-con}$  and  $Z_{d-con}$  respectively but circumventing  $Z_{con}$ . The goal is to divert the passing-trips to  $Path_{alter}$  to avoid  $Z_{con}$ , thus to alleviate the traffic congestion inside  $Z_{con}$ . To this end, all the distinct paths ( $Path_{odr}$ ,  $r=1 \dots Num_{od}$ ) with  $Z_o=Z_{o-con}$  and  $Z_d=Z_{d-con}$ , obtained from  $TP(Z_o, Z_d, r, TimeP, Day, DayT)$ , are visualized (on the travel-pattern-layer). Among these paths, the ones that do not traverse  $Z_{con}$  are selected (if there is existence of such paths), and the corresponding values ( $M_{odr}$ ,  $V_{odr}$ ,  $L_{odr}$  and  $T_{odr}$ ) are listed in an attribute window. The path with the shortest travel time (or distance) is subsequently chosen as the alternative route  $Path_{alter}$  (See Fig. 3).

### 3.6.2 Other possible ways to further alleviate the congestion in $Z_{con}$

If  $Path_{alter}$  is not found, i.e. if all trips between  $Z_{o-con}$  and  $Z_{d-con}$  have passed  $Z_{con}$ , this suggests that the congestion zone  $Z_{con}$  is critical for linking the corresponding OD zones, and that the traffic situations in the surrounding area of  $Z_{con}$  leave less (acceptable) choices for drivers to take other routes. It is likely that among all the potential routes between  $Z_{o-con}$  and  $Z_{d-con}$ , the current path  $Path_{od-con}$  (e.g. provided by a route planner) has the shortest travel time (or distance). In contrast, the other routes (if exist) may take too much longer travel time or distances than  $Path_{od-con}$  to be considered by travelers. In this case, an in-depth examination into the specific road situations surrounding  $Z_{con}$  is conducted, and the matrix  $RL(Z_i, Z_j, Z_l, TimeP, Day, DayT)$  is utilized. The analysis focuses on the following aspects. (1) The road linkage ( $M_{ijl}$  and  $V_{ijl}$ ) in *the surrounding-area of  $Z_{con}$*  consisting of  $Z_{con}$  and its geographically adjacent zones, (2) the mismatch between the road connections and major sources of the flows, and (3) the possible new routes that could be generated in order to replace the current travel path.

## 4 The case study

### 4.1 The data and study region

The data are provided by a large logistic company in Greece which monitors the travel of more than 6,500 utility vehicles across the country via GPS devices installed in the vehicles. The devices collect information at an average rate of 0.48 *minutes* (min), generating data of 1.07GB each day and 1.1TB over three years. A range of variables is collected, including vehicle positions (e.g. GPS coordinates and recording time), drivers' driving patterns (e.g. instant speeds and headings), and vehicle conditions (e.g. engine status and fuel levels). The study region is *Attica Basin*, the conglomeration of Greek cities of Athens and Piraeus as well as their suburban areas, with a population of over 3.5 million inhabitants. According to the report (Tuszyńska 2018), logistics has been a core sector for economic growth of this region, manifested by a high number of utility vehicles, i.e. 120 vehicles per 1000 residents. Accordingly, the data cover approximately 1.5% of the total fleet of this area. In this study, the data of 3 months between September and November of 2018 are used, and the total size of the data is 86.4GB. The adopted variables include vehicle ids, GPS coordinates and time, and instant speeds.

### 4.2 The VAA and SAA components

While a range of VAA (e.g. Robinson 2017) and SAA (e.g. R and Python) tools can be utilized for the analysis, in this study the two components are implemented by means of *V-Analytics* (the Geospatial Visual Analytics) and *SAS* (the Statistical Analysis System), respectively. *V-Analytics* (Andrienko et al. 2013a) is a software package composed of a set of comprehensive functionalities, realizing a number of state-of-the-art visual analytic approaches. It provides both a basic platform and more advanced techniques for interactively analyzing mobility data and extracting knowledge from the data. *SAS* is a software suite for advanced analytics; it accommodates a multitude of classical and modern statistical and data management approaches. Its architecture designs enable the system to scale up to perform efficient analysis on large sizes of data (e.g. Pope 2017).

### 4.3 GPS data preprocessing and trip extraction

From all the experimental data, a sample dataset, consisting of 1,300 (20% of the total) vehicles for a regular week with 1.3GB in size, is generated. The examination into the sample data identified the following data problems. Approximately 0.08% of the points have the coordinate  $X_k$  or  $Y_k$  as zero, 1.14% have the instant speed  $v_k$  higher than 130 m/h (the highest driving speed limit in Greece), and 0.04% have duplicates of the same point IDs and time stamps (i.e.  $id_k=id_{k+1}$  and  $t_k=t_{k+1}$ ).

Moreover, problems were also revealed regarding the time intervals between consecutive points. Fig. 4 describes the distribution of the intervals. It was noted that, while the average is 0.48 min (the typical data recording rate), the intervals vary over a range of 0-3 min, with the highest peak at 0.1 min. However, a second peak at 2 min was also observed, accounting for 2% of the total intervals. Further investigation shows that this peak is mainly caused by points that appear either at highways with some intermediate points being not recorded (e.g. due to bad satellite connections) or *at the border of the study area*. The latter phenomenon occurred when data for the study area are extracted from a larger dataset covering a more extended territory. To extract data from the larger dataset, the data provider just used a rectangle delimiting the study area and removed all GPS points that lie beyond this area. This leads to specific cases of data missing when vehicles temporarily move out of the enclosed area and return back after a few minutes, making artificially long time intervals of two consecutive points that consist of the last position before moving out and first position after returning back. Thus, the points with time intervals longer than (or equal to) 2 min and the OD trips that contain such points are both considered as errors.

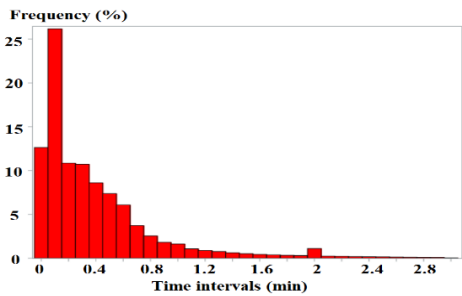


Fig. 4 Distribution of the time intervals between consecutive points

Based on the above detected problems, the following rules are extracted: (1)  $X_k \neq 0$  and  $Y_k \neq 0$ ; (2)  $v_k \leq 130 \text{ km/h}$ ; (3) if  $id_k = id_{k+1}$  and  $t_k = t_{k+1}$ ,  $p_{k+1}$  is deleted; and (4) if  $t_{k+1} - t_k \geq 2 \text{ min}$ ,  $p_{k+1}$  is deleted.

In the trip extraction, suitable settings for  $TH_{Act}$  and  $TH_{Trip}$  depend on the research questions. In this study,  $TH_{Act}$  is set as 3 min and  $TH_{Trip}$  as 100 meters. This is based on the data examination as well as the study (Cich et al. 2016) in which optimal values for  $TH_{Act}$  and  $TH_{Trip}$  are decided through the comparison between trips derived from GPS data and those recorded in the corresponding travel diaries (as ground-truth data). Under the former value, a stop for longer than 3 min is considered as a stop-location for activities (e.g. parcel deliveries); while according to the latter, the movement longer than 100 meters in distance is regarded as a trip with clear destinations (thus reflecting travel patterns). These parameter values, along with the extracted rules, are applied to the entire dataset for data cleaning and trip derivation in SAA. Each of the derived trips is further examined; if the original GPS trace of the trip contains consecutive points with the time intervals not less than 2 min, the trip is removed. Finally, 5.1 million trips were derived from a total of 91 days, with 8.63 trips on average for each vehicle each day.

The left and right of Fig. 5 describe the distributions of the average of  $v_k$  and the average number of points per half an hour over all the weekdays, respectively. From the left figure, clear variations in driving speeds across different time periods of the day were revealed, leading to the splitting of a day into 7 periods, including 7-9am, 9-10:30am, 10:30am-15pm, 15-17pm, 17-19pm, 19-21pm, and 21pm-7am. The average speed in each of these periods is 35.6, 37.4, 34.2, 38.8, 40.8, 37.8, 43.7 (km/h), respectively. According to the right figure, the average number of points over the above-obtained periods is 19.2%, 20.5%, 22.7%, 20.6%, 10.8%, 6.0% and 0.2%, respectively. Large differences in travel demand are demonstrated among these time periods, underlying the causes for the observed speed deviations.

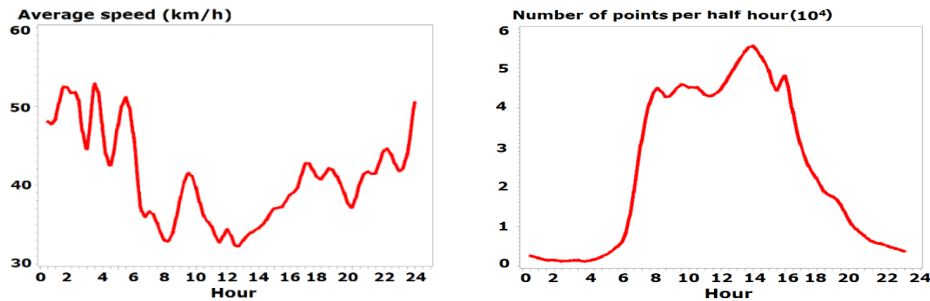


Fig. 5 Distributions of the average of  $v_k$  (left) and average number of points (right) over each half an hour

#### 4.4 Traffic condition, road linkage and travel pattern matrices

##### 4.4.1 Division of the study area

The study area is located in the range of longitude (19.870, 26.587) and latitude (35.046, 41.479). During the construction of matrices, the entire area is divided into zones; *Grid\_X* and *Grid\_Y* decide the total number of the study units. The larger these values are, the higher the spatial resolution reaches, but the less the number of observed GPS points in each zone and between zones. In order to derive results that are statistically sound and representative, these two variables are set as 400 respectively, resulting in a total of  $1.6 \times 10^5$  zones with each being  $1.62 \text{ km}^2$  in size. When this size is compared to other existing studies, it was noted that the average size of the units varies depending on study areas and travel modes. It ranges from  $2.14 \text{ km}^2$  in the Twin Cities for car-based transport analysis (Anderson et al. 2013), to  $0.15 \text{ km}^2$  in Denizli of Turkey for transit studies (Gulhan et al. 2013), and to  $0.03 \text{ km}^2$  and  $0.05 \text{ km}^2$  in two towns of Sweden for traffic studies on a combination of bikes and autos (Makr  and Folkesson, 1999).

##### 4.4.2 The matrices

Based on the spatial partition, along with the previously-defined 7 temporal periods, three matrices are built, including the traffic-condition-matrix  $TC(Z_i, \text{TimeP}, \text{Day}, \text{DayT})$ , road-linkage-matrix  $RL(Z_i, Z_j, Z_l, \text{TimeP}, \text{Day}, \text{DayT})$ , and travel-pattern-matrix  $TP(Z_o, Z_d, r, \text{TimeP}, \text{Day}, \text{DayT})$ .  $Z_i, Z_j, Z_l, Z_o$  and



$Z_d$  represent zones, with  $i, j, l, o, d=1 \dots 400$ ;  $TimeP=1 \dots 7$ ;  $Day=1 \dots 91$  (all the data collection days); and  $DayT=weekdays, weekends$  and  $public\ holidays$ . A range of variables is derived from the matrices, including the total number of segments ( $M_i$ ) in  $Z_i$  and average travel speed ( $V_i$ ) of the segments; the total number of segments ( $M_{ijl}$ ) successively passing  $Z_i, Z_j$  and  $Z_l$  and average speed ( $V_{ijl}$ ) of the segments; the total number of distinct travel paths ( $Num_{od}$ ) between  $Z_o$  and  $Z_d$ , the  $r^{th}$  ( $r=1 \dots Num_{od}$ ) specific path ( $Path_{odr}$ ), the number of trips ( $M_{odr}$ ) along the path, and the average travel speed ( $V_{odr}$ ), distance ( $L_{odr}$ ) and time ( $T_{odr}$ ) over the trips. Between different time periods of the day or different types of days, traffic conditions in each zone or between zones could differ to a large extent. In the following, the traffic in the morning (7-9am) of weekdays is analyzed, but the same process can be repeated to the remaining periods and day types. The procedure is identical, but the results are likely to be different.

Fig. 6 demonstrates the visualization of  $TC$  for a part of the study area. Each zone  $Z_i$  (on the middle panel) is described as a rectangle (a grid), and the values of the variables (*attributes*)  $M_i$  and  $V_i$  of the zone are represented by different colours of the grid lines or area. *Conditions* on each single attribute or on the combination of multiple attributes can be specified, such that only the zones that satisfy these conditions are shown (e.g. the zones with  $V_i < 20\text{km/h}$  being visualized in Fig. 6). From the displayed zones, one can be further selected, and the specific attribute values of the zone are presented in an *attribute window*. On the left panel, the color scheme is described; on the right, the scheme can be re-defined. In this study, only relevant visualization elements are introduced; more details about V-Analytics can be referred to in the literature (Andrienko et al. 2013a).

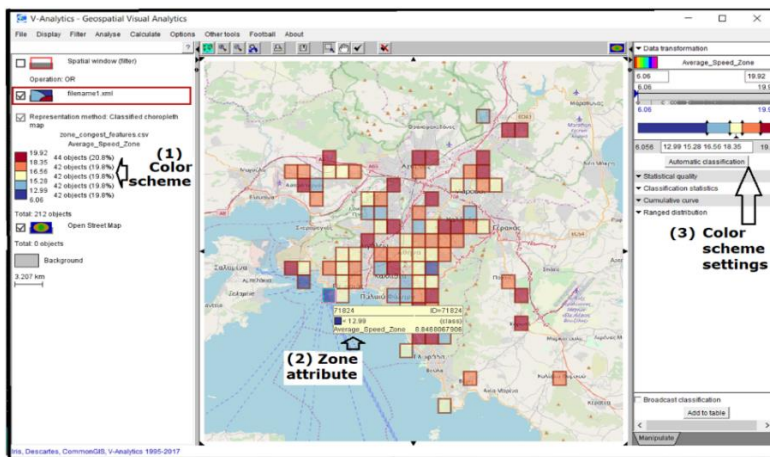


Fig. 6 Visualization of the traffic-condition-matrix  $TC$  (traffic-condition-layer)

Note: on the middle panel, each grid represents a zone, with the color of the grid area reflecting the categories of  $V_i$  of the zone. The small (attribute) window indicates the original value of  $V_i$  for the selected zone.

Fig. 7 describes the visualization of  $RL$ , on which road connections in the surrounding-area of a selected zone  $Z_i$  (i.e.  $Z_{224,189}$ , labelled as  $Z_{ij}$  in the black grid) are shown. This (surrounding) area consists

of  $Z_i$  and its eight adjacent zones (labelled as  $Z_{i,j}$ , with  $i-1 \leq i' \leq i+1$  and  $j-1 \leq j' \leq j+1$ ). Fig. 7a shows road connections that start from the study zone  $Z_{i,j}$ , while Fig. 7b-7f illustrate the connections that begin from each of five (out of the eight) surrounding zones, including  $Z_{i-1,j}$ ,  $Z_{i+1,j}$ ,  $Z_{i-1,j+1}$ ,  $Z_{i,j+1}$  and  $Z_{i+1,j+1}$  respectively. On each of these figures, the zone where the connections start is highlighted in the purple grid, and the connection among three zones is expressed as a curve that starts and ends in the first and last zones respectively while passing the second zone. Take the connection  $Z_{i,j} \rightarrow Z_{i,j-1} \rightarrow Z_{i+1,j-1}$  in Fig. 7a as an example, the purple curve describes the connection that begins from the small green circle in  $Z_{i,j}$ , passes  $Z_{i,j-1}$  and ends at the end (arrow) of this curve in  $Z_{i+1,j-1}$ . The colour and/or thickness of the curve reflects the average speed ( $V_{ijl}$ ) and/or the number of trips ( $M_{ijl}$ ) along the connected roads. Apart from the black and purple grids, the red grids represent the congestion zones (detected in Section 3.5).

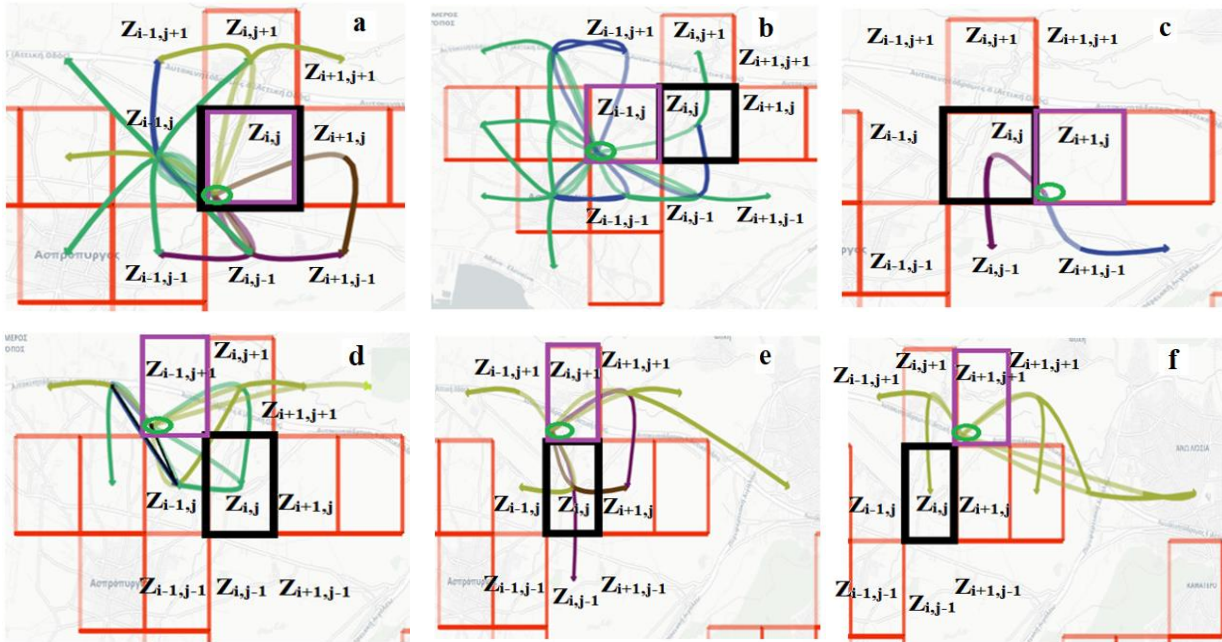


Fig. 7 Visualization of the road-linkage-matrix  $RL$  in the surrounding-area of  $Z_{i,j}$  (road-linkage-layer)  
 Note: the black, purple and red grids denote the selected zone  $Z_{i,j}$  (i.e.  $Z_{224,189}$ ), the zone where the connections start, and the congestion zones, respectively. Each curve describes the connection among 3 zones, starting from the green circle in the 1<sup>st</sup> zone, passing the 2<sup>nd</sup> zone, and ending at the end of the curve in the 3<sup>rd</sup> zone. The color of the curve reflects  $V_{ijl}$  of the roads.

From Fig. 7, road connections starting from a zone and variations in the connections across zones were observed. For example, there are only 2 connections starting from  $Z_{i+1,j}$  (Fig. 7c), while 15 and 7 connections originating from  $Z_{i-1,j}$  (Fig. 7b) and  $Z_{i,j+1}$  (Fig. 7e) respectively. However, despite multiple connections from a certain zone, there could be lack of roads in certain directions, e.g. no connections of  $Z_{i-1,j} \rightarrow Z_{i-1,j+1} \rightarrow Z_{i,j+1}$  in Fig. 7b or  $Z_{i,j+1} \rightarrow Z_{i-1,j+1} \rightarrow Z_{i-1,j}$  in Fig. 7e. Furthermore, the three zones involved in a connection may not be geographically adjacent; there could be intermediate zones in between, e.g.  $Z_{i-1,j+1} \rightarrow Z_{i+1,j+1} \rightarrow Z_{i+2,j+1}$  (Fig. 7d),  $Z_{i,j+1} \rightarrow Z_{i+1,j+1} \rightarrow Z_{i+4,j}$  (Fig. 7e), and  $Z_{i+1,j+1} \rightarrow Z_{i+3,j} \rightarrow Z_{i+5,j}$  (Fig. 7f),

with the zone  $Z_{i-1,j+1}$ , zones  $Z_{i+2,j+1}$  and  $Z_{i+3,j}$ , and zones  $Z_{i+2,j}$  and  $Z_{i+4,j}$  being skipped respectively. This is resulted from two consecutive GPS points that skip one (or a few) (geographically adjacent) zone(s) in between these points, indicating of a high likelihood that travel speeds of the points are high and that the connected roads are featured with a high speed limit. Further investigation discloses that there is indeed a highway going through the neighbouring zones  $Z_{i-1,j+1}$ ,  $Z_{i,j+1}$  and  $Z_{i+1,j+1}$ .

All the above observations demonstrate the ability of Fig. 7 in depicting road network situations in the surrounding-area of a selected (congestion) zone  $Z_{i,j}$ . This information, combined with the major traffic sources of the congestion zone (as displayed in Fig. 11 and 12), becomes an important tool for the identification of mismatch between traffic flows and road network services surrounding the congestion area, enabling further examination into the traffic problems. This will be elaborated in Section 4.7.2.

Fig. 8 illustrates the visualization of  $TP$ , on which travel patterns between a selected zone pair  $Z_o$  and  $Z_d$  are displayed as curves representing all the travel paths (i.e.  $Path_{odr}$ ,  $r=1 \dots Num_{od}$ ) between the corresponding zones. The colour and/or thickness of the curves reflect the values of the travel speed ( $V_{odr}$ ), distance ( $L_{odr}$ ) and/or travel time ( $T_{odr}$ ) along these paths.

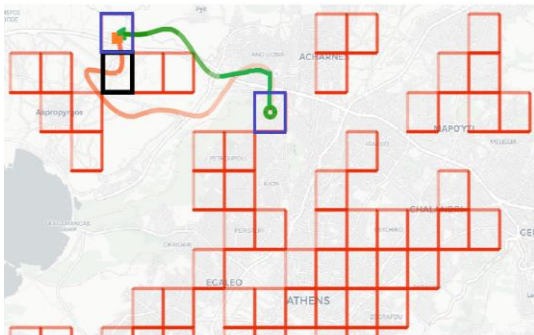


Fig. 8 Visualization of the travel-pattern-matrix  $TP$  (travel-pattern-layer)

Note: the purple grids are the selected origin and destination zones  $Z_{229,188}$ , and  $Z_{224,190}$  respectively, and the black grid is  $Z_{224,189}$ . The curves represent all the (two) travel paths between the OD zones, with the color denoting the travel speed.

#### 4.5 Congestion zone detection

In the detection,  $TH_{mz}$ ,  $TH_{vz}$  and  $TH_{con}$  are designated as 40 20km/h and 0.8 respectively, based on the literature (Cui et al. 2016a; Zheng et al. 2011) in combination with the data sampling rate and number of sampling vehicles in the experimental data. This leads to 184 zones being filtered out as the congestion zones. These places have undertaken at least 40 trips in the morning per weekday, and suffered from the average travel speeds lower than 20km/h at least for 4 in 5 of the days. Fig. 9 describes the geographic distribution of all the congestion zones.

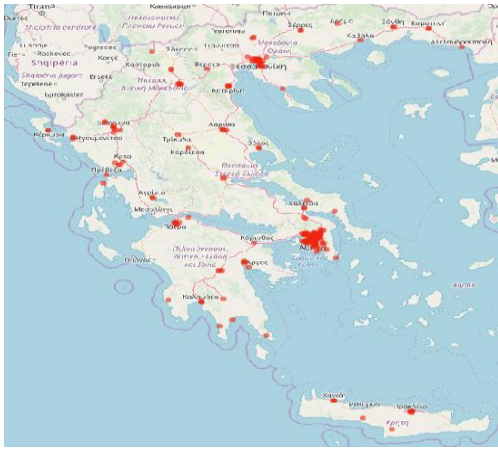


Fig. 9 Geographic distribution of all the congestion zones in the study area (congestion-zone-layer)  
 Note: each red grid represents a congestion zone

#### 4.6 Major sources of traffic flows in the congestion zones

To analyse traffic flows in the congestion zones, a typical congestion zone  $Z_{224,189}$  was used as demonstration. This zone is located in the commercial area of Athens, and the average speed and number of trips in the morning each day in this area are 18.6km/h and 201.9, respectively. All the morning trips over all the 65 experimental weekdays are generated by 380 distinct OD pairs. Among these trips 20.5% both start and end in  $Z_{224,189}$ , 13.9% and 21.9% only start or end in this zone, and the remaining 43.7% just pass this area.

Let  $TH_{od-con}=0.05$ , 8 OD pairs (2.1% of all the ODs) are filtered out; trips between each of these pairs contribute to at least 5% of the total flows in  $Z_{224,189}$ . Table 1 presents these ODs, and Fig. 10 further illustrates the common path ( $Path_{od-con}$ ) for each of these ODs. From these figures, it was noted that the major traffic sources in  $Z_{224,189}$  are from the west to this zone (Fig. 10c and 10g), from this zone to the east (Fig. 10d), from the east through this zone to the west (Fig. 10e and 10f) or to the north (Fig. 10h), and from the north through this zone to the southeast (Fig. 10i).

Table 1 Major sources of traffic flows in  $Z_{224,189}$ \*

| OD-ID | $Z_{o-con}$ | $Z_{d-con}$ | $Path_{od-con}$   | $M_{od-con}$ | Flow          |
|-------|-------------|-------------|---|--------------|---------------|
| 1     | 224,189     | 224,189     | <b>(224,189)-(224,189)</b>  | 20.5%        | Start and end |
| 2     | 221,189     | 224,189     | (221,189)- <b>(224,189)</b>   | 10.4%        | End           |
| 3     | 224,189     | 225,189     | <b>(224,189)</b> -(225,189)   | 7.1%         | Start         |
| 4     | 237,188     | 221,189     | (237,188)-(237,187)-(236,187)-(236,186)-(235,187)-(234,187)-(234,188,)-(233,188)-(232,188)-(231,188)-(230,188)-(230,189)-(229,189)-(228,189)-(227,189)-(226,190)-(225,190)-(224,190)- <b>(224,189)</b> -(223,189)-(222,189)-(221,189) | 6.5%         | Pass          |
| 5     | 232,186     | 221,189     | (232,186,)-(232,187)-(233,187)-(232,188)-(231,188)-(230,188)-(230,189)-(229,189)-(228,189)-(228,189)-(227,189)-(226,190)-(225,190)-(224,190)- <b>(224,189)</b> -(223,189)-(222,189)-(221,189)   | 5.3%         | Pass          |
| 6     | 223,189     | 224,189     | (223,189)- <b>(224,189)</b>   | 5.3%         | End           |
| 7     | 229,188     | 224,190     | (229,188)-(229,189)-(228,189)-(227,188)-(226,188)-(225,188)-(224,188)-(223,189)- <b>(224,189)</b> -(224,190)  | 5.1%         | Pass          |

|   |         |         |   |      |      |
|---|---------|---------|---|------|------|
| 8 | 224,190 | 230,183 | (224,190)-(224,189)-(223,189)-(223,188)-(222,188)-(222,187)-(222,186)-(223,186)-(223,185)-(224,185)-(225,185)-(226,185)-(227,185)-(227,184)-(228,184)-(229,184)-(229,183)-(230,183) | 5.0% | Pass |
|---|---------|---------|---|------|------|

\*: the columns from the left to right represent the id of the OD pair, origin zone, destination zone, common travel path, number of trips between the OD zones, and direction of the flows. Zones are identified with the grid numbers in the longitude and latitude dimensions respectively. The study zone (224,189) ( $Z_{224,189}$ ) is in bold.

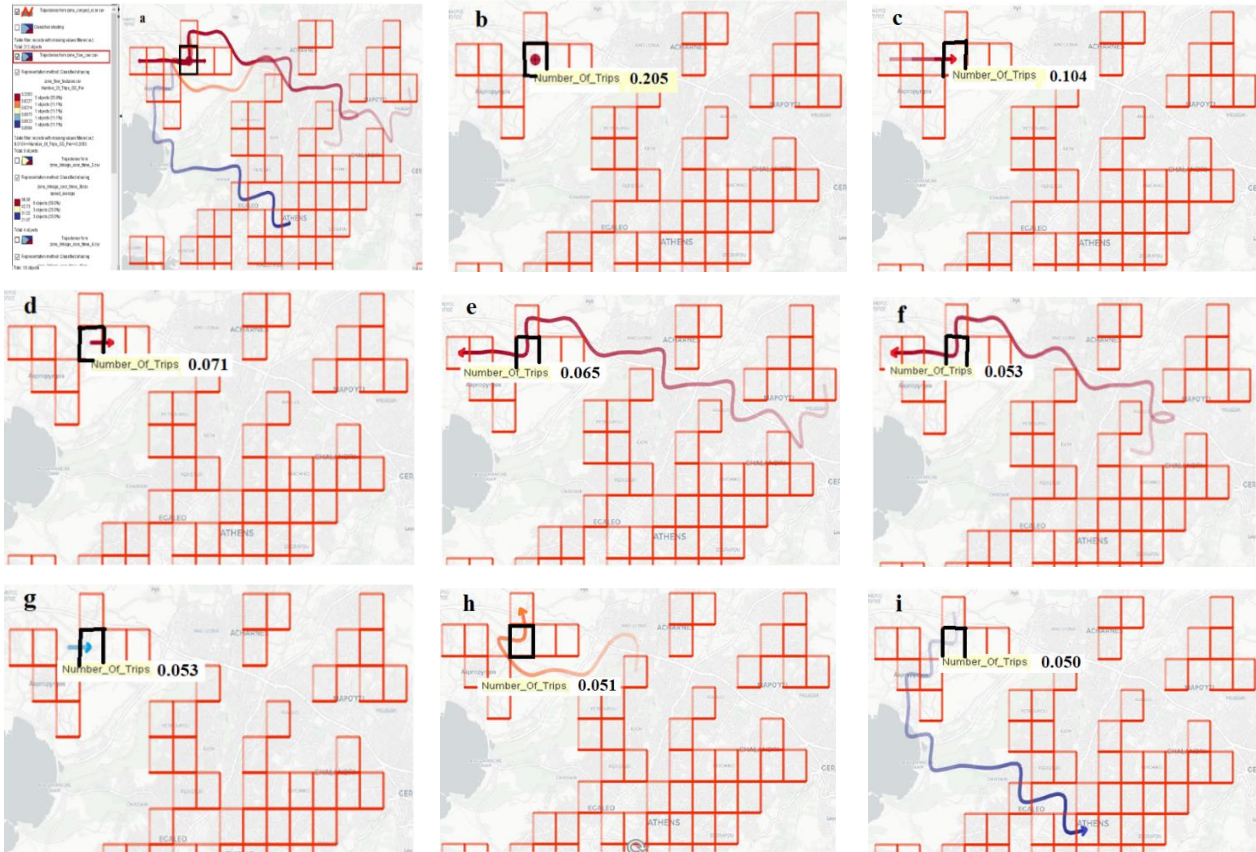


Fig. 10 Major sources of traffic flows in  $Z_{224,189}$  (travel-flow-layer)

Note: the black and red grids are  $Z_{224,189}$  and congestion zones, respectively. The curve describes the typical path  $Path_{od-con}$  and the attribute window lists the value of  $M_{od-con}$ . Fig. a displays all the 8 paths and Fig. b-i depicts each of these paths.

#### 4.7 Specific transport situations and possible ways of reducing congestion in $Z_{224,189}$

##### 4.7.1 Alternative routes

Out of all the major sources listed in Table 1, four (i.e.  $OD-ID \in \{4, 5, 7, 8\}$ ) have passed  $Z_{224,189}$ . The examination into the trips discloses that only one of these sources, i.e.  $OD-ID=7$  from  $Z_{229,188}$  to  $Z_{224,190}$  ( $Path_{od-con} = Z_{229,188} - Z_{229,189} - Z_{228,189} - Z_{227,188} - Z_{226,188} - Z_{225,188} - Z_{224,188} - Z_{223,189} - Z_{224,189} - Z_{224,190}$ ) (Fig. 10h), has one additional travel route that bypasses  $Z_{224,189}$ . This path, i.e.  $Path_{odr} = Z_{229,188} - Z_{229,189} - Z_{228,189} - Z_{227,189} - Z_{226,190} - Z_{225,190} - Z_{224,190}$ , is subsequently chosen as the alternative route ( $Path_{alter}$ ) that could replace the original path. Fig. 8 describes this route (the curve in green), and the orange curve on this figure is the original path ( $Path_{od-con}$ ) that traverses  $Z_{224,189}$ .

The comparison between  $Path_{alter}$  and  $Path_{od-con}$  delimits the following differences (Table 2). (1)  $Path_{alter}$  has a lower average speed (28.3km/h) but shorter travel distance (10.9km) than  $Path_{od-con}$  featured with the speed and travel distance as 35.4m/h and 12.7km respectively. (2) Both routes are mainly comprised of roads with high speed limits. However, due to heavy traffic in the morning rush hour, the average speeds of both routes do not reach their limits. Particularly, the part of  $Path_{od-con}$  inside  $Z_{224,189}$  suffers from heavy congestion and low driving speeds (i.e. the average speed of 18.6km/h), leading to the overall travel time of  $Path_{od-con}$  as 21.5 min. In contrast, although the whole travel time is 23.1 min (1.6 min longer than  $Path_{od-con}$ ),  $Path_{alter}$  has a stable traffic condition along this path, with the average speed at each zone passed being higher than 20km/h. (3) Regardless of the above differences, more people have taken  $Path_{od-con}$  than  $Path_{alter}$ , with the average number of trips per day as 10.3 (83.7%) along  $Path_{od-con}$  but only 2 (16.3%) through  $Path_{alter}$ .

Table 2 Comparison between the original path and the alternative route

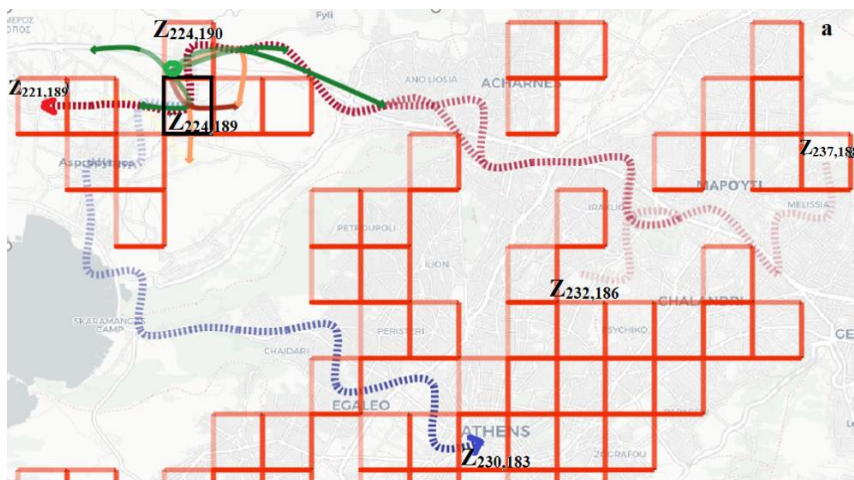
| Route           | Number of zones passed | Number of congestion zones passed | Route distance (km) | Average speed (km/h) | Travel time (min) | Number of trips per day |
|-----------------|------------------------|-----------------------------------|---------------------|----------------------|-------------------|-------------------------|
| $Path_{alter}$  | 5                      | 0                                 | 10.9                | 28.3                 | 23.1              | 2 (16.3%)               |
| $Path_{od-con}$ | 7                      | 1                                 | 12.7                | 35.4                 | 21.5              | 10.3 (83.7%)            |

To have a further look into the traffic situations of the two paths, additional analysis is performed on the off-peak period of 9-10:30am when the average driving speed is 37.4km/h (See Fig. 5). During this period, the speed of  $Z_{224,189}$  increases to 22.9km/h. The traffic conditions of both  $Path_{alter}$  and  $Path_{od-con}$  have also improved, with the average speeds as 47.4km/h and 57.5km/h respectively. This leads to the travel time as 13.8 and 13.3 min, and the numbers of trips per day as 3.1 (39.7%) and 4.7 (60.3%), respectively. Thus, in relation to the morning rush hour,  $Path_{alter}$  is more closed to  $Path_{od-con}$  in terms of travel time (only 0.5 min in difference) and  $Path_{alter}$  also undertakes more trips (23.4% more) in the off-peak period.

From the above analysis, it was noted that the majority (83.7% and 60.3%) of travelers between the OD zones (from  $Z_{229,188}$  to  $Z_{224,190}$ ) adopt the original path  $Path_{od-con}$  instead of  $Path_{alter}$  (during 7-9am and 9-10:30am respectively). Apart from shorter travel time (1.6 min and 0.5 min shorter), there could be other factors contributing to the route choice (e.g. poor connectivity between the high-speed road and local roads inside  $Z_{229,188}$  or  $Z_{224,190}$  along the path  $Path_{alter}$ ). Moreover, given that the experimental data are generated from utility vehicles for logistic purposes, the route patterns may not be representative of all trips between the OD zones. Private trips may exhibit different route choices from the observed ones. Thus, before any management decisions (e.g. replacing  $Path_{od-con}$  with  $Path_{alter}$  under certain enforcement measures) are made, detailed inspection should be conducted regarding why  $Path_{od-con}$  is preferred to  $Path_{alter}$  and what is the representability of the observed route patterns.

#### 4.7.2 Other possible ways to alleviate the congestion

For the remaining three sources (i.e.  $OD-ID \in \{4,5,8\}$ ) that pass  $Z_{224,189}$ , no other trips have been observed between the corresponding OD zones that circumvent the congestion zone. Fig. 11a describes these sources (in the red and blue dash curves), which are from  $Z_{237,188}$  to  $Z_{221,189}$ , from  $Z_{232,186}$  to  $Z_{221,189}$ , and from  $Z_{224,190}$  to  $Z_{230,183}$ , respectively, accounting for 16.8% of the total flows in  $Z_{224,189}$ . The road connections (7 in total) starting from  $Z_{224,190}$  on the road-linkage-layer (described in Fig. 7e) is also displayed (in the green, red and orange solid curves). From the zoomed-in map in Fig. 11b, it was observed that the connections begin from  $Z_{224,190}$  and go to the northwest, northeast, southeast and south respectively. However, no road connections are present towards the direction of the southwest, i.e.  $Z_{224,190} \rightarrow Z_{223,190} \rightarrow Z_{223,189}$  (*the missing-link*) (shown in the black curve). This causes all the trips from these three sources taking the connection  $Z_{224,190} \rightarrow Z_{224,189} \rightarrow Z_{223,189}$  (i.e. traversing  $Z_{224,189}$  in order to reach  $Z_{223,189}$  from  $Z_{224,190}$ ). Due to the missing-link, mismatch is formed between the road connectivity (among the three zones  $Z_{224,190}$ ,  $Z_{223,190}$  and  $Z_{223,189}$  in the corresponding direction) and these major flows. Further inspection reveals that there are roads available in the area of these zones (shown in the black circle), including a highway and several local roads. But there is lack of connections between the highway and local roads inside  $Z_{223,190}$ . These roads are only linked in a further area of  $Z_{222,190}$ . This leads to none of the trips of these sources choosing the highway and local roads in order to get to  $Z_{223,189}$  from  $Z_{224,190}$  while avoiding  $Z_{224,189}$  (i.e. none of the trips taking the connection  $Z_{224,190} \rightarrow Z_{223,190} \rightarrow Z_{222,190} \rightarrow Z_{223,189}$ ). Thus, if new roads (shown in the black arrow) were built to connect the highway and local roads inside  $Z_{223,190}$ , the missing-link ( $Z_{224,190} \rightarrow Z_{223,190} \rightarrow Z_{223,189}$ ) could be generated, enabling these major flows to be diverted from the original connection ( $Z_{224,190} \rightarrow Z_{224,189} \rightarrow Z_{223,189}$ ) to the new link, therefore bypassing  $Z_{224,189}$ .



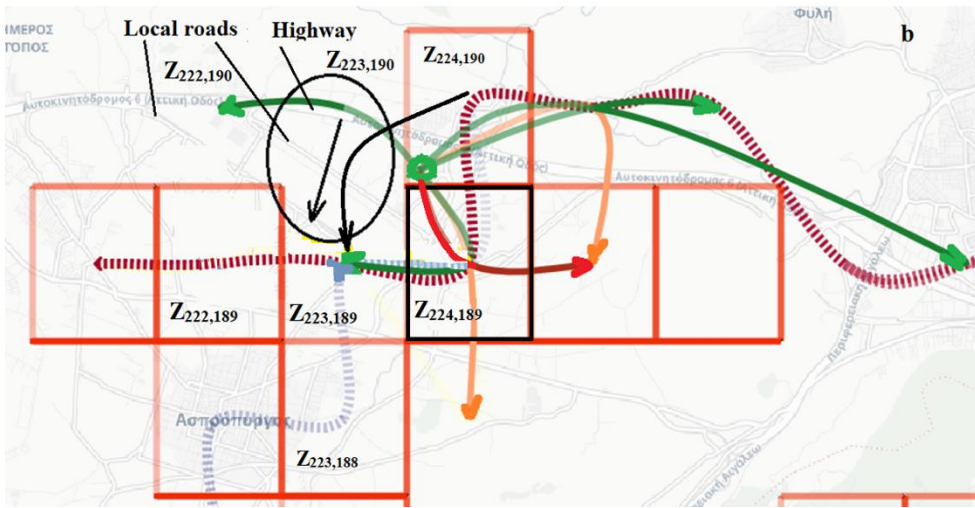
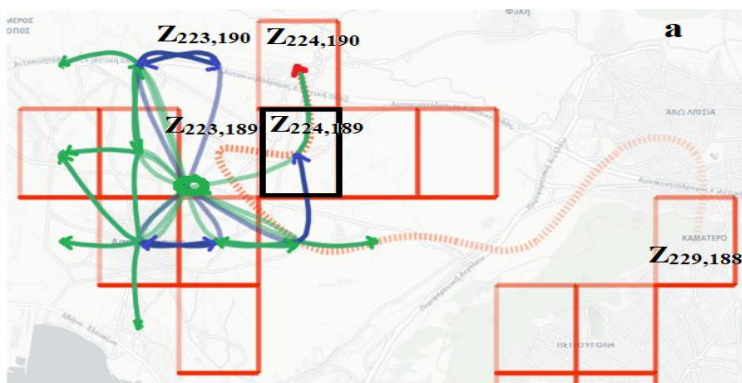


Fig. 11 The three major sources and the road linkage starting from  $Z_{224,190}$

Note: on both a and b, the black grid represent  $Z_{224,189}$ , the dash curves in red and blue are the major traffic sources, and the solid curves in green, red and orange are the road connections starting from  $Z_{224,190}$ . The black curve, circle and arrow on b denote the missing-link, the area containing the mismatch, and the proposed new road, respectively.

Similar situations occur to the source of  $OD-ID=7$ . Apart from the alternative route identified in Section 4.7.1, there could be other ways to divert the corresponding trips. Fig. 12a and 12b demonstrate this source (in the red dash curve from  $Z_{223,189}$  to  $Z_{224,190}$ ); the road linkage starting from  $Z_{223,189}$  (depicted in Fig. 7b) is also shown. It was noticed that, despite various (15 in total) connections from  $Z_{223,189}$ , an important connection towards the northeast is missing, i.e.  $Z_{223,189} \rightarrow Z_{223,190} \rightarrow Z_{224,190}$  (the missing-link) (represented in the black curve in Fig. 12b). This leads to the corresponding trips passing  $Z_{224,189}$  in order to reach  $Z_{224,190}$  from  $Z_{223,189}$  (i.e. taking the connection  $Z_{223,189} \rightarrow Z_{224,189} \rightarrow Z_{224,190}$ ). Like in Fig. 11b, mismatch exists in the opposite direction of the road connectivity among the three zones  $Z_{223,189}$ ,  $Z_{223,190}$  and  $Z_{224,190}$  (Fig. 12b). If new roads (denoted in the black arrow) were constructed connecting the highway and the local roads inside  $Z_{223,190}$ , the missing-link ( $Z_{223,189} \rightarrow Z_{223,190} \rightarrow Z_{224,190}$ ) could be created, enabling the trips to take the route along the new link, thus avoiding  $Z_{224,189}$ .





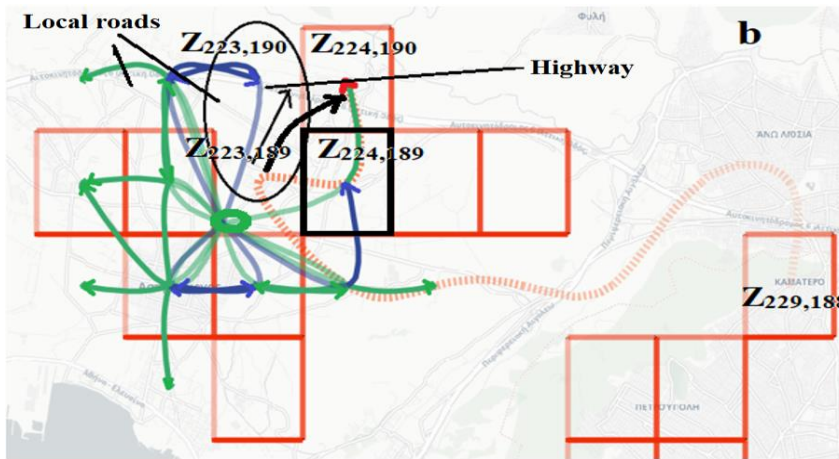


Fig. 12 The major source of OD-ID=7 and the road linkage starting from  $Z_{223,189}$

Note: on both a and b, the black grid represent  $Z_{224,189}$ , the red dash curve is the source, and the solid curves in green and blue are the road connections starting from  $Z_{223,189}$ . The black curve, circle and arrow on b refer to the missing-link, the area for the mismatch, and the proposed new road, respectively.

## 5 Discussions and conclusions

Due to the rapid development of technologies, an extensive growth in big mobility data exists and is continuously expanding. These technologies offer a solution to the challenges associated with conventional travel data. However, obtaining significant mobility knowledge from the data and using the knowledge for supporting traffic management decisions require detailed but efficient data analysis as well as good communication and exploration of results. Towards this perspective, this paper has developed a method for citywide traffic analysis based on the combination of visual and analytical approaches. Applications to large volumes of GPS data have demonstrated the potential and effectiveness of the approach in achieving such a goal.

The method and the results that arise in this study will help traffic managers improve the understanding of current traffic (e.g. through the traffic-condition-layer, travel-pattern-layer and congestion-zone-layer), its major sources (through the traffic-flow-layer), and mismatch between traffic flows and road network services (through the road-linkage-layer). Based on the results, further investigation can be performed in order to design more effective policy measures. To this end, the proposed method does not only identify traffic problems, but more importantly, it provides a platform (by means of the traffic-condition-map) to assist managers in further exploring these problems and making appropriate decisions. Particularly, through the combination of the traffic-flow-layer and travel-pattern-layer (e.g. in Fig. 8), alternative routes ( $Path_{alter}$ ) that start and end in the same places as the OD zones ( $Z_{o-con}$  and  $Z_{d-con}$ ) of the major traffic source of a congestion zone ( $Z_{con}$ ) can be identified. Moreover, by overlaying the traffic-flow-layer and road-linkage-layer (e.g. in Fig. 11 and 12), mismatch between road connectivity and major sources of traffic flows in  $Z_{con}$  is revealed. Based on the mismatch, possible

ways (e.g. new roads) could be further suggested in alleviating the traffic problems. Note that all the above analysis is performed in the VAA component, allowing interactive inspection into the traffic situations, facilitating managers gaining more insights into the problems and discoveries of new policy measures. Moreover, all the visualized results are derived from large volumes of GPS data, ensuring more objective and representative of the detected problems, laying a basis for the design of more effective measures.

A number of areas lies ahead for future improvement. Firstly, the traffic situations (e.g. the average speed  $V_i$  and major traffic source  $Path_{od-con}$  of a congestion zone, and the travel pattern  $Path_{odr}$  between two zones) could be dynamically visualized over the course of a day based on temporal information (e.g. across different time periods). Secondly, in this study the transport situations concerning only passing-trips (e.g.  $OD-ID \in \{4,5,7,8\}$ ) are examined and the ways of diverting the trips are investigated. Further work should be done regarding the other major sources that start or end in (rather than passing) the congestion zone  $Z_{con}$ . The goal is not to divert the trips from  $Z_{con}$ , but to examine if the capacity of the road connections between  $Z_{con}$  and its adjacent zones (e.g. the connections  $Z_{224,189} \rightarrow Z_{225,189}$  in Fig. 10b and  $Z_{223,189} \rightarrow Z_{224,189}$  in Fig. 10c and 10g) sufficiently serve these major flows. Thirdly, out of all the congestion zones detected in the study area, 45 (21.2% of the total) are geographically distributed as single ones, 57 (26.7%) have 2 or 3 congestion zones connected, and the rest (51.9%) form large congestion areas with more than 3 zones (most of which are in the city center). In this study, only a single congestion zone is analyzed. In the future, the method could be applied to a larger place consisting of multiple congestion zones.

Fourthly, in the method a variety of parameters has been defined; the performance of the approach thus depends on the specification of these parameters, particularly the following ones. (1) The minimum duration ( $TH_{Act}$ ) and distance ( $TH_{Trip}$ ) above which a stop and a trip are selected respectively, (2) the number of zones ( $Grid\_X$  and  $Grid\_Y$ ) of the study area, (3) the minimum number of trip segments ( $TH_{mz}$ ), lowest speed in normal conditions ( $TH_{vz}$ ), and smallest probability ( $TH_{con}$ ) which determine whether a zone is considered as experiencing congestion, and (4) the minimum percentage ( $TH_{od-con}$ ) of trips between a pair of OD, above which the pair is selected as a major source of the traffic in  $Z_{con}$ . In specifying these parameters, higher values of  $TH_{Act}$  and  $TH_{Trip}$  would miss activities for short duration (e.g. parcel deliveries) and trips with short distances (e.g. between geographically closed locations), but lower values may pick up non-activities (e.g. stops at traffic lights) and non-trips (e.g. movement under bridges), respectively. Furthermore, the combination of higher values of  $Grid\_X$ ,  $Grid\_Y$ ,  $TH_{mz}$ ,  $TH_{con}$  and  $TH_{od-con}$  and lower values of  $TH_{vz}$  would lead to the derived results in a more detailed spatial resolution, more statistically representative, and the detection of more severe congestion problems. But

the stricter parameter values also call for more GPS data, thus requiring a higher data sampling rate and/or more sampling vehicles. In future research, investigation should be conducted regarding how and to what extent the derived results are influenced by these parameters and what is the minimum amount of GPS data needed for various combinations of the parameter values. This will provide an important guideline for the parameter selection issue.

Fifthly, in deriving the travel distance of a trip segment, the *geodetic distance* ( $d_{mn}$ ) is used, which is the sum of the geographic distance ( $D(p_k, p_{k+1})$ ) between two adjacent GPS points along the path (See Formula 1). The geodetic distance has also been adopted in a number of studies (e.g. Cui et al. 2016b; Zheng et al. 2011) to estimate distances of trips based on GPS data. When this distance is compared with the *network distance* (i.e. the length of the shortest path between two locations along the transport network), the former is fast and easy to compute, while the latter requires more time and complex analysis due to the utilization of network analysis techniques and geographic information systems (e.g. Cubukcu and Taha 2016; Okabe et al 2006). Moreover, further examination into the experimental data reveals that the average difference between  $D(p_k, p_{k+1})$  and the actual distance of the adjacent points (after map-matching to specific roads) is 0.014km, leading to the deviation between the average speed (derived from  $D(p_k, p_{k+1})$ ) and the actual speed of the two points as 1.75km/h (given the data sampling rate of 0.48 min). This suggests that the actual speeds are typically 1.75km/h higher than the derived results, including  $v_{mn}$  (Formula 1),  $V_i$  (Formula 2),  $V_{ijl}$  (Formula 3) and  $V_{odr}$  (Formula 4), and that the actual threshold  $TH_{vz}$  for congestion detection is 1.75km/h higher than the designated value (20km/h). Thus, while geodetic and network distances produce different absolute values, they do not affect much the detection of congestion (i.e. with the actual threshold  $TH_{vz}$  being increased by a certain amount). The use of geodetic distances can generate sufficiently accurate results (Ivis 2006; Zheng et al. 2011); the higher the data sampling rate, the closer the two distances, and the more accurate the results are. Nevertheless, in order to obtain even more precise results, the network distance could be considered in the future, as the transport network topology varies across different areas. The results could be compared to the ones in the current study, and variations between them could be delimited.

Lastly, the method primarily focuses on systematically examining traffic conditions across the urban area, with the goal of uncovering traffic problems that are persistent over a long time. Due to the volume of the GPS data utilized and the scale of the analysis, the method is normally implemented off-line. However, the approach could also be applied to real-time analysis on a local area (in small sizes), through the construction and visualization of the matrices ( $TC$ ,  $RL$  and  $TP$ ) and the detected congestion zones (alongside their major traffic sources) in this area for a short period (e.g.  $TimeP=5$  or 10 min) of the current day. Due to the small size and short time interval, the amount of data being analysed is

considerably reduced, leading to the update of the computed results and corresponding map layers in a short time (e.g. 5 or 10 min), enabling near real-time analysis.

## 6 References

- Andrienko G, Andrienko N, Bak P, Keim D, Wrobel S (2013a) *Visual Analytics of Movement*, Springer
- Andrienko G, Andrienko N, Hurter C, Rinzivillo S, Wrobel S (2013b) Scalable analysis of movement data for extracting and exploring significant places. *IEEE transactions on visualization and computer graphics*, 19(7):1078-1094. <https://doi.org/10.1109/TVCG.2012.311>
- Andrienko G, Andrienko N, Fuchs G (2016) Understanding movement data quality. *journal of location based services*, 10(1):31-46. <https://dx.doi.org/10.1080/17489725.2016.1169322>
- Andrienko G, Andrienko N, Chen W, Maciejewski R, Zhao Y (2017) Visual analytics of mobility and transportation: state of the art and further research directions. *IEEE Transactions on Intelligent Transportation Systems*, 18(8): 2232-2249. <http://dx.doi.org/10.1109/TITS.2017.2683539>
- Batty M (2013) *The New Science of Cities*. MIT Press
- Chae JH, Thom D, Jang Y, Kim SY, Ertl T, Ebert DS (2014) Public behaviour response analysis in disaster events utilizing visual analytics of microblog data. *Computers & Graphics*, 38:51–60
- Chen S, Andrienko G, Andrienko N, Doukeridis C, Koumparos A (2019) Contextualized Analysis of Movement Events. *EuroVis Workshop on Visual Analytics (2019)*
- Cich G, Knapen L, Bellemans T, Janssens D, Wets G (2016) Threshold settings for TRIP/STOP detection in GPS traces. *J Ambient Intell Human Comput* 7: 395-413
- Cubukcu KM, Taha H (2016) Are Euclidean Distance and Network Distance Related? *Asia-Pacific International Conference on Environment-Behavior Studies*, Edinburgh University 2016. DOI: 10.21834/e-bpj.v1i4.137
- Cui JX., Liu F, Hu J, Janssens D, Wets G, Cools M (2016a). Identifying mismatch between urban travel demand and transport network services using GPS data: A case study in the fast growing Chinese city of Harbin. *Neurocomputing*, 181, 4–18
- Cui JX, Liu F, Janssens D, An S, Wets G, Cools M (2016b) Detecting urban road network accessibility problems using taxi GPS data. *Journal of Transport Geography*, 51: 147–157
- Dias KL , Pongelupe MA, Caminhas WM, de Errico L (2019) An innovative approach for real-time network traffic classification. *Computer Networks*, 158: 143–157
- Itoh M, Yokoyama D, Toyoda M, Tomita Y, Kawamura S, Kitsuregawa M (2016) Visual exploration of changes in passenger flows and tweets on mega-city metro network. *IEEE Trans, Big Data*, 2(1): 85–99. <https://doi.org/10.1109/TBDDATA.2016.2546301>

- Ivis F (2006) Calculating geographic distance: Concepts and methods. Proc. 19th Conf. Northeast SAS User Group 2006
- Lansley G, Longley P (2016) The geography of twitter topics in London, Computers, Environment and Urban Systems, 58:85-96. <https://doi.org/10.1016/j.compenvurbsys.2016.04.002>
- Liu H, Jin SC, Yan YY, Tao YB, Lin H (2019) Visual analytics of taxi trajectory data via topical sub-trajectories. Visual Informatics, 3:140–149
- Markovic N, Sekula P, Vander Laan Z, Andrienko G, Andrienko N (2019) Applications of trajectory data from the perspective of a road transportation agency: literature review and maryland case study. IEEE Transactions on Intelligent Transportation Systems. <http://dx.doi.org/10.1109/TITS.2018.2843298>
- Okabe A, Okunuki KI, Shiode S. (2006). The SANET toolbox: new methods for network spatial analysis. Transactions in GIS, 10(4): 535-550
- Robinson A (2017) Geovisual Analytics. The Geographic Information Science & Technology Body of Knowledge (3rd Quarter 2017 Edition), John P. Wilson (ed.). doi: 10.22224/gistbok/2017.3.6
- Ruan ZY, CSong CC, Yang XH, Shen GJ, Liu Z (2019) Empirical analysis of urban road traffic network: A case study in Hangzhou city, China. Physica A, 527:121287
- Skupin A (2013) A visual exploration of mobile phone users, land cover, time, and space. Pervasive and Mobile Computing, 9: 865–880
- Thomas J, Cook K (2005) Illuminating the Path: The research and Development Agenda for Visual Analytics. IEEE
- Tuszyńska B (2018) Transport and Tourism in Greece. Directorate-General for Internal Policies of the Union. Publications Office of the European Union. <https://publications.europa.eu/en/publication-detail/-/publication/ced95429-6548-11e8-ab9c-01aa75ed71a1>
- Xie C, Li MK, Wang HY, Dong JY (2019) A survey on visual analysis of ocean data. Visual Informatics, 3: 113–128
- Yuan NJ, Zheng Y, Zhang LH, Xie, X (2011) T-Finder: A Recommender System for Finding Passengers and Vacant Taxis, Proceedings of the 13th ACM international conference on Ubiquitous computing (UbiComp 2011)
- Zeng JW, Qian YS, Yu SB, Wei XT (2019) Research on critical characteristics of highway traffic flow based on three phase traffic theory. Physica A, 530:121567
- Zheng Y, Liu YC, Yuan J, Xie X (2011) Urban Computing with Taxicabs. UbiComp'11, Beijing, China.